JOURNAL OF MATERIALS SCIENCE 26 (1991) 1749–1754

Corrosion of silicon nitride ceramics under hydrothermal conditions

T. SATO, T. MURAKAMI, T. ENDO, M. SHIMADA
Department of Molecular Chemistry and Engineering, Faculty of Engineering, Tohoku University, Sendai 980, Japan

K. KOMEYA, T. KAMEDA, M. KOMATSU
New Material Engineering Laboratory, Toshiba Corporation, 2-4 Suehiro-Cho, Tsurumi-Ku, Yokohama 230, Japan

Corrosion behaviour of Si_3N_4 ceramics containing Y_2O_3, Al_2O_3 and AlN as sintering aids was investigated under hydrothermal conditions at 200–300 °C and saturated vapour pressures of water for 1–10 days. Hydrothermal corrosion resulted in the dissolution of the Si_3N_4 matrix and the formation of a product layer consisting of the original grain-boundary phases and hydrated silica. The dissolution rate of Si_3N_4 ceramics decreased with decreasing crystallinity of the grain-boundary phase. The dissolution rate could be adequately described by a parabolic plot in the initial stage of the reaction. The apparent activation energies were 83.5–108 kJ mol^{-1}, and the bending strength of the corroded samples decreased from $\sim$ 600 to 400 MPa in the initial stage of the reaction upto a weight loss of 0.004 g cm^{-2}, and then was almost constant up to a weight loss of 0.012 g cm^{-2}.

1. Introduction

Silicon nitride ceramics have received attention for structural applications because of their excellent physical and chemical properties, such as high fracture strength, fracture toughness, thermal shock resistance, chemical stability, etc. Many studies on the corrosion behaviour of Si_3N_4 ceramics at high temperature, such as in molten salts or gas environments, have been conducted, but few studies at moderate temperature have been performed. Because Si_3N_4 ceramics are generally fabricated by using additives such as MgO, Y_2O_3, Al_2O_3, AlN, etc. as sintering aids, these additives form grain-boundary phases in Si_3N_4. The physical and chemical properties of Si_3N_4 ceramics depend significantly on the amounts of the grain-boundary phases and also their degree of crystallization [1]. In previous studies [2, 3], we reported that Si_3N_4 ceramics suffered serious corrosive attack in aqueous HF and HCl solutions at moderate temperature below 100 °C. The corrosion rate and the degradation behaviour of the fracture strength of Si_3N_4 ceramics in these acidic solutions greatly depended on the crystallinity of the grain-boundary phases [2, 3]. On the other hand, Yoshimura *et al.* [4, 5] and Yoshio *et al.* [6–8] reported that Si_3N_4 ceramics suffered corrosive attack under hydrothermal conditions. The corrosion reaction is suspected to proceed as shown by Equation 1 [4].

$$Si_3N_4 + 6H_2O = 3SiO_2 + 4NH_3 \quad (1)$$

Because the solubility of SiO_2 greatly increases at hydrothermal conditions [9], Si_3N_4 ceramics show noticeable weight loss. It was reported [6–8] that the degree of the dissolution of Si_3N_4 ceramics under hydrothermal conditions depended on the kind of additives used and the morphology of the Si_3N_4 grain. However, no information concerning the effect of crystallinity of the grain-boundary phase on the corrosion behaviour has reported. In the present study, a series of tests was conducted to examine the effect of the crystallinity of the grain-boundary phase on the corrosion behaviour of the Si_3N_4 ceramics containing Y_2O_3, Al_2O_3 and AlN as sintering aids.

2. Experimental procedure

Pressureless sintered Si_3N_4 containing about 3.5 wt % Y^{3+} and 3 wt % Al^{3+} as Y_2O_3,.Al_2O_3 and AlN were used as corrosion test samples. The crystallinity of the grain-boundary phase was determined by X-ray diffraction analysis using a graphite crystal, monochromatic CuK_α radiation (50 kV at 80 mV) [1]. The grain-boundary phases in these Si_3N_4 ceramics was quantitatively determined as crystal, a mixture of crystal and glass, and glass. These samples were denoted as SN–1, SN–2, and SN–3, respectively, and the characteristics of the samples are summarized in Table I.

All samples were cut into rectangular coupons, 2 mm × 5 mm × 20 mm and were polished to a mirror-like surface. In each corrosion test, weighed specimens and desired amounts of distilled water were sealed in a stainless steel autoclave. The amount of distilled water, V (cm^3), was determined as V/A

0022–2461/91 $03.00 + .12

TABLE I Characteristics of the samples

Sample	Additive		Grain-boundary phase	Density ($g\,cm^{-3}$)	σ_{3b} (MPa)	K_{IC} ($MPa\,m^{1/2}$)	H_v (GPa)	E (GPa)	Dimension (mm^3)
	Y (wt %)	Al (wt %)							
SN–1	3.5	3.4	Crystal	3.22	670	6.0	16.0	237	2 × 5 × 13
SN–2	3.6	2.7	Crystal + glass	3.23	605	6.6	15.7	232	2 × 5 × 11
SN–3	3.6	2.4	Glass	3.22	530	5.7	14.9	209	2 × 5 × 12

= 20 cm, where A (cm^2) was the sum of the initial surface area of samples. The autoclave was then placed in an electric furnace regulated at the desired temperature. In the present study, the temperature varied from 200–300 °C and the pressure was set at the saturated vapour pressure of water at each temperature. After keeping at the desired temperature and time, the autoclave was removed from the electric furnace and cooled. The sample was then removed from the autoclave and dried. The degree of dissolution of the sample was determined by the weight loss of the sample. The crystalline phase of the corroded sample was determined by X-ray diffraction analysis (XRD) using Ni-filtered CuK_α radiation and the microstructures of samples were observed by scanning electron microscopy (SEM). The bending strength of the sample was determined by the three-point bending test with a span length of 10 mm and a crosshead speed of 0.5 mm min^{-1}.

3. Results and discussion

The weight loss (W/A) of various Si_3N_4 ceramics under hydrothermal conditions at 200–300 °C for 3 days is shown in Fig. 1, where W is the weight loss and A is the initial surface area of the sample. Significant weight loss was observed in all samples. The degree of the dissolution of the samples was in the order of SN–1 > SN–2 ≫ SN–3. These results indicated that the dissolution rate of Si_3N_4 ceramics under hydrothermal conditions increased with increasing crystallinity of the grain-boundary phase.

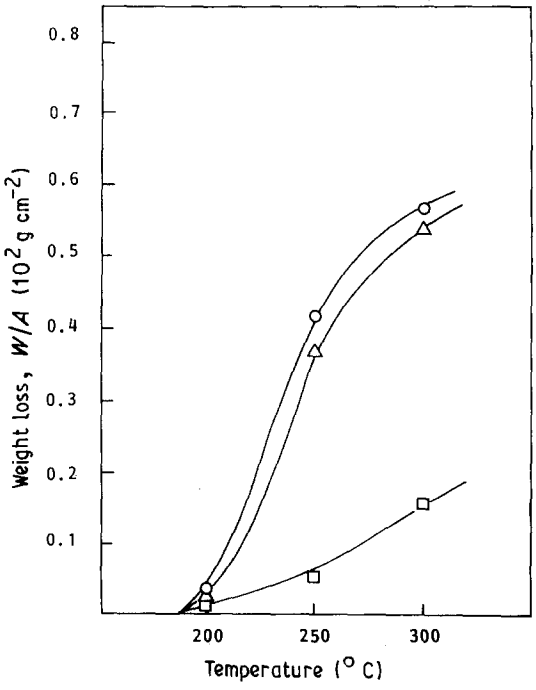

Figure 1 The weight loss of various Si_3N_4 ceramics under hydrothermal conditions at 200–300 °C and saturated water vapour pressure for 5 days. (○) SN–1, (△) SN–2, (□) SN–3.

The samples were blackish before hydrothermal corrosion, but were coated with thin layer of white product after the corrosion. Scanning electron micrographs of the surfaces and cross-sections of SN–1 and SN–3 corroded under hydrothermal conditions at 300 °C for 5 days are shown in Fig. 2. The corrosion products uniformly coated the surface of the samples. The thickness of the corrosion products on the surface of SN–1 and SN–3 were ~ 15 and 8.5 μm, respectively. As seen in the scanning electron micrographs, the inner corrosion products formed on the surface of SN–1 consisted of fine grains of ~ 1 μm, but plate-like compounds were also formed on the surface. On the other hand, the corrosion products formed on the surface of SN–3 uniformly consisted of fine grains.

X-ray diffraction patterns of the surfaces of SN–1 and SN–3 samples before and after corrosion at 300 °C for 5 and 10 days are shown in Fig. 3. Because no noticeable change in XRD pattern was observed in SN–3 samples, it is considered that the corrosion products which accumulated on the surface were amorphous to X-rays. On the other hand, XRD peaks corresponding to the grain-boundary phase [1] became stronger after corrosion of SN–1 samples. These results indicated that the corrosion rate of the Si_3N_4 matrix was faster than that of the grain-boundary phase, and the grain-boundary phase was consequently concentrated in the corrosion product layer on the surface of the sample.

Infrared absorption spectra of the Si_3N_4 powder and the corrosion products formed on the surfaces of SN–1 and SN–3 by hydrothermal corrosion at 300 °C and 8.6 MPa for 10 days, are shown in Fig. 4. Infrared spectra of both the corrosion products were quite different from that of the Si_3N_4 sample. No noticeable difference was observed in the infrared spectra of the products formed on the surfaces of SN–1 and SN–3. The absorption peaks corresponding to Si–O stretching and Si–O bending mode were observed at 1030 and 520 cm^{-1}, respectively. The absorption peaks at 1620 and 3500 cm^{-1} might be attributed to H–O bending and H–O stretching, respectively. Absorption peaks corresponding to N–H bending vibration of NH_4^+ adsorbed on the surface possessing Si–OH [6, 10] were also observed at 1400 cm^{-1}. Therefore, it was suspected that the corrosion products which formed on the surface of Si_3N_4 consisted of hydrated

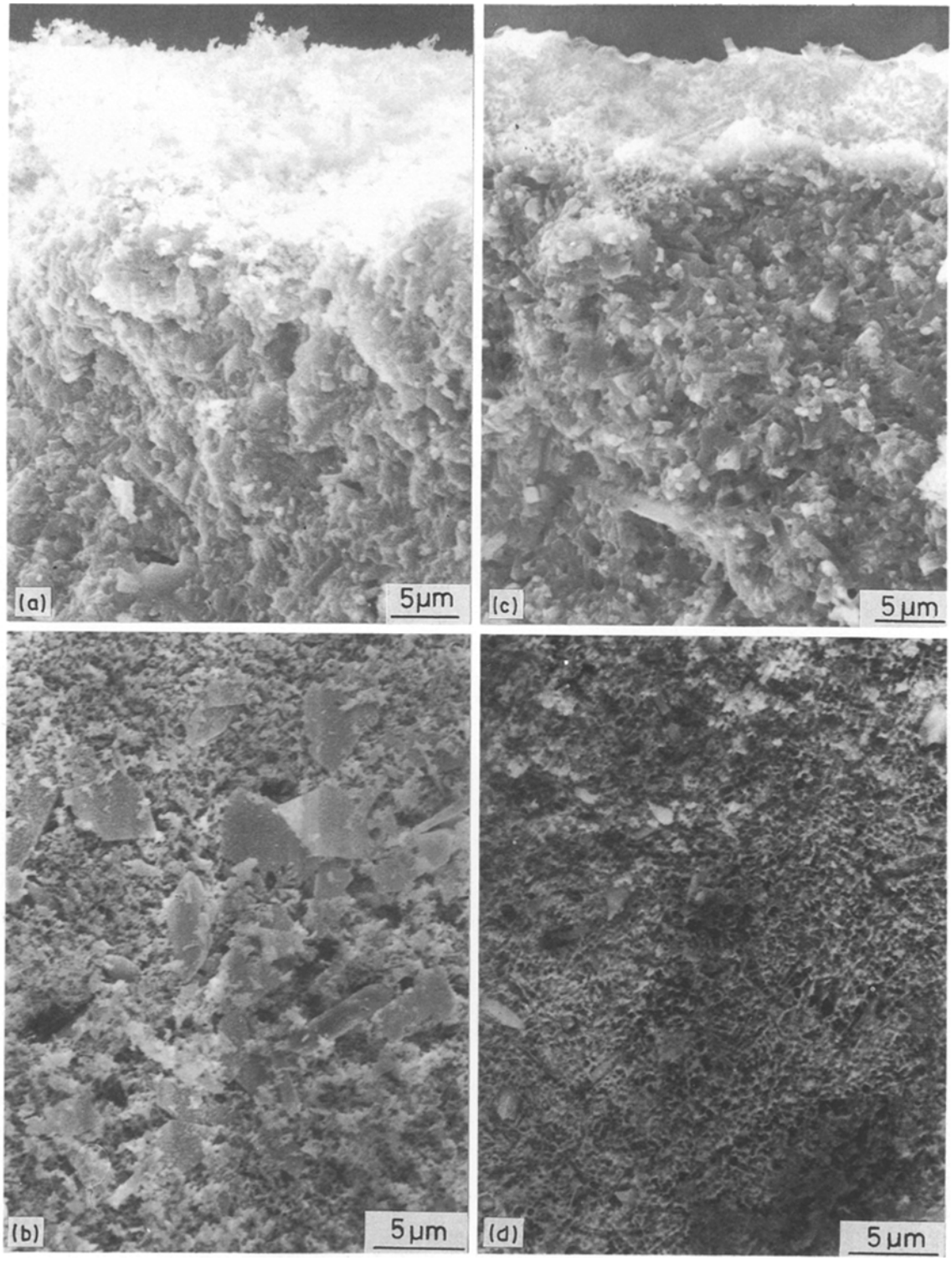

Figure 2 Scanning electron micrographs of the surfaces and the cross-sections of (a, b) SN–1 and (c, d) SN–3 corroded under hydrothermal conditions at 300 °C and 8.6 MPa for 5 days. (a, c) Cross-sections of corroded SN–1 and SN–3. (b, d) Surfaces of corroded SN–1 and SN–3.

silica adsorbing NH_4^+ together with the original grain-boundary phases.

The time dependence of the weight loss for various Si_3N_4 samples corroded under hydrothermal conditions at various temperatures is shown in Fig. 5. The rate of dissolution at 200 °C decreased with time as expected for the diffusional control reaction through the product layer. However, the corrosion rate at 300 °C increased rapidly in the final stage of the reaction. A similar phenomenon was observed in the reaction at 250 °C for the samples showing large weight loss, such as SN–1 and SN–2. These results might be interpreted as the separation of the product layers from the surface of samples. From these results, it was suspected that the corrosion reaction was depressed by the formation of the product layer, but the product layer broke away from the sample after growing thick. Therefore, the corrosion rate of the samples were determined by the parabolic plots shown by Equation 2 in the initial stage of the reactions

$$(W/A)^2 = kt \quad (2)$$

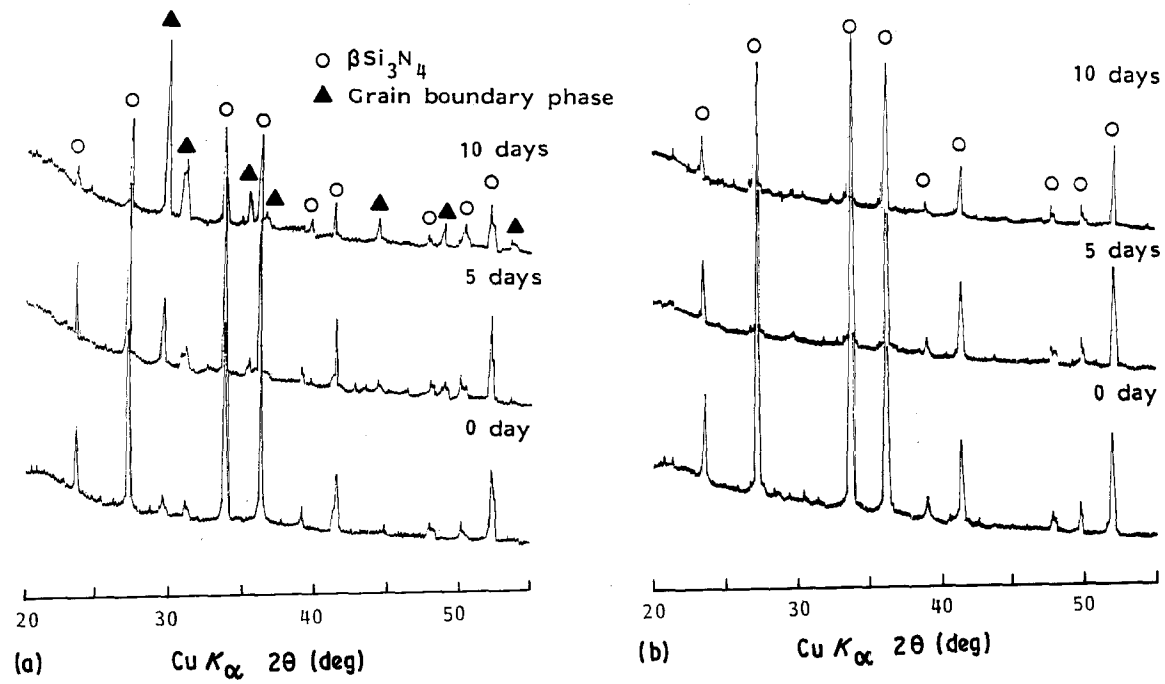

Figure 3 X-ray diffraction patterns of the surfaces of (a) SN–1 and (b) SN–3 before and after corrosion at 300 °C and 8.6 MPa for 5 and 10 days. (○) β-Si_3N_4, (▲) grain-boundary phase.

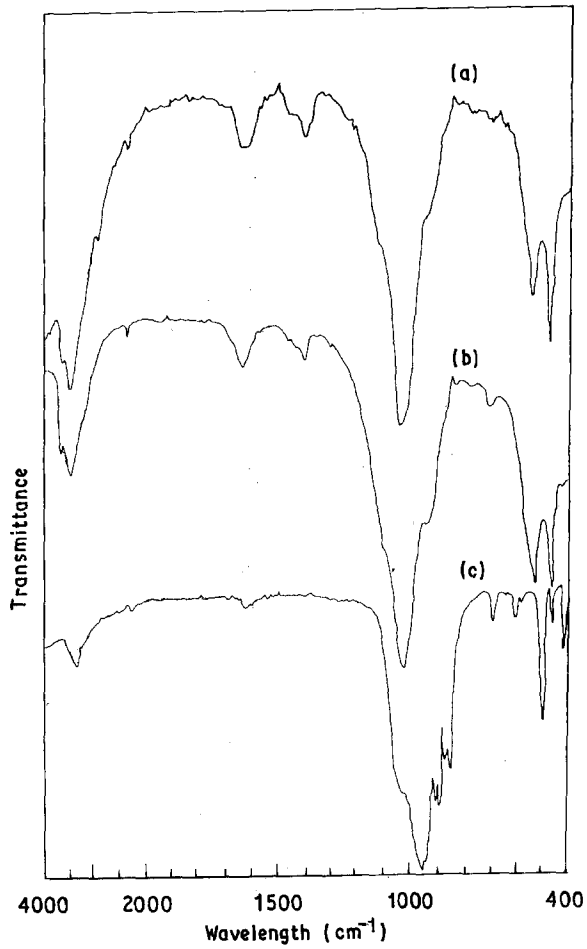

Figure 4 Infrared absorption spectra of the corrosion products formed on the surfaces of (a) SN–1 and (b) SN–3 by hydrothermal corrosion at 300 °C and 8.6 MPa for 10 days; (c) that of Si_3N_4.

where k is the rate constant and t is time. The results are shown in Fig. 6. Some spread was seen in the data at 300 °C for SN–1 and SN–2, but the data of other samples were adequately described by the parabolic plots. From the slopes of these straight lines, the corrosion rate constants, k, were determined. The Arrhenius plots of the corrosion rate constant are shown in Fig. 7. The apparent activation energies were 83.5–108 kJ mol^{-1}. These values were almost the same as that for diffusion of H_2O through amorphous SiO_2 reported by Burn and Roberts [11]. Therefore, it was suspected that the hydrothermal corrosion of Si_3N_4 ceramics was controlled by the diffusion of H_2O through the product layer.

The bending strength of the corroded samples under hydrothermal conditions at 200–300 °C are shown in Fig. 8 as a function of the weight loss. The bending strength of all samples decreased from ~ 600–400 MPa until causing 0.004 g cm^{-2} weight loss and then almost constant up to 0.012 g cm^{-2} weight loss under the present reaction conditions. These results indicated that the flaws about 2.5 times larger than the original critical flaws were introduced in the initial stage of the corrosion reaction and then the flaw sizes were almost constant. No noticeable difference in the strength degradation behaviour was observed in these samples possessing different crystallinity of the grain-boundary phase. Therefore, the crystallinity of the grain-boundary phase seemed to affect only the dissolution rate of the Si_3N_4 matrix under hydrothermal conditions.

4. Conclusions

1. Hydrothermal corrosion of Si_3N_4 ceramics resulted in the dissolution of the Si_3N_4 matrix and the

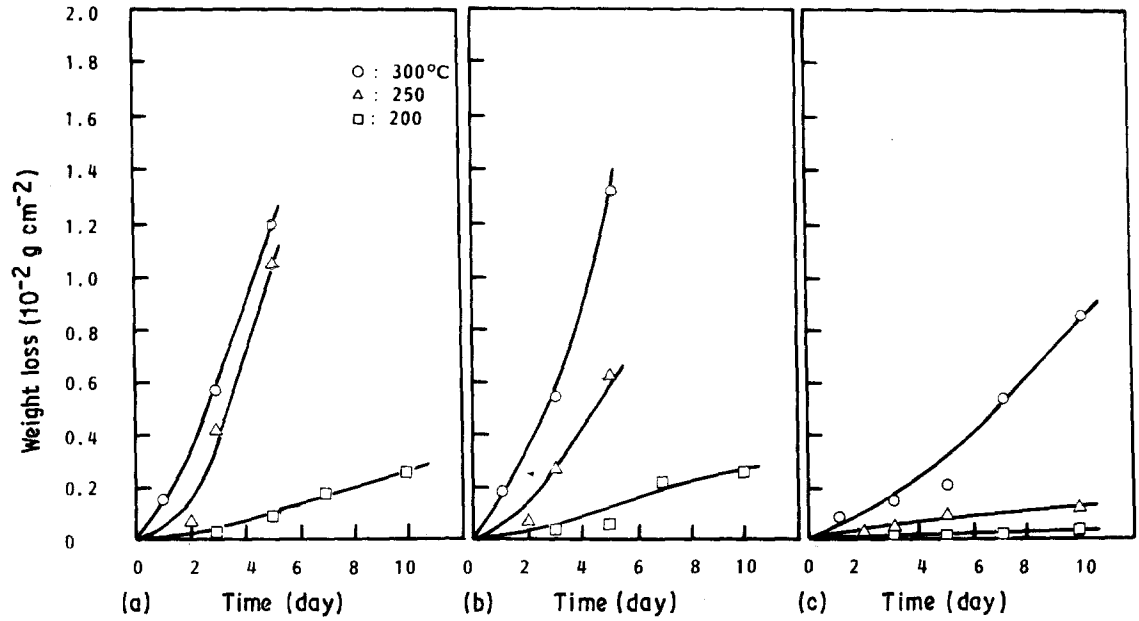

Figure 5 Time dependence of the weight loss for various Si_3N_4 ceramics under hydrothermal conditions at various temperatures. (a) SN–1, (b) SN–2, (c) SN–3. (□) 200 °C, (△) 250 °C, (○) 300 °C.

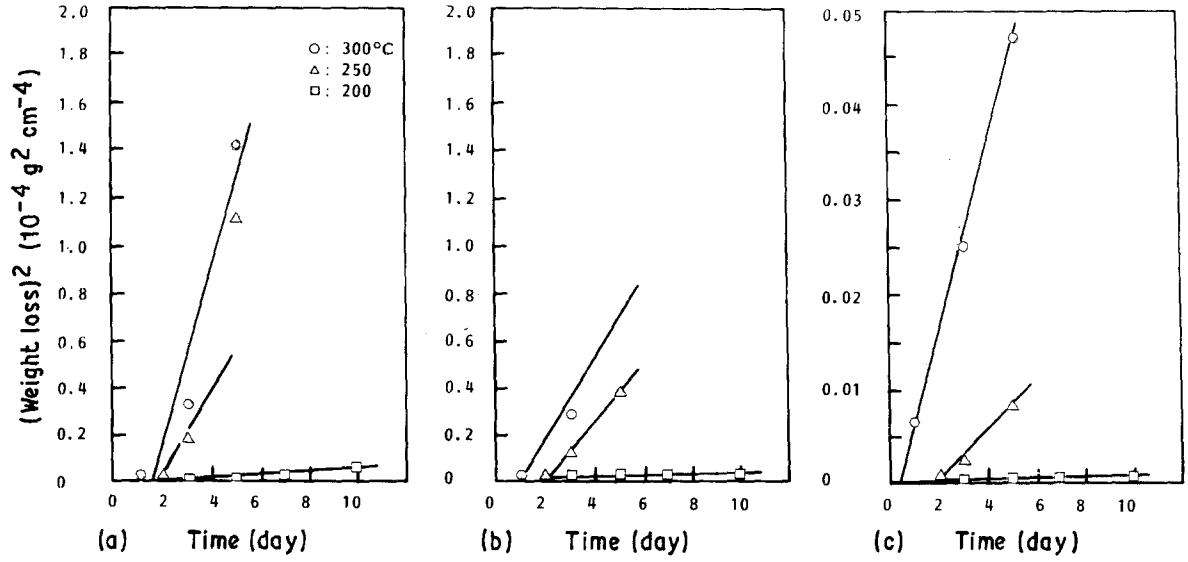

Figure 6 Parabolic plots of the hydrothermal corrosion data of various Si_3N_4 ceramics. (a) SN–1, (b) SN–2, (c) SN–3. (□) 200 °C, (△) 250 °C, (○) 300 °C.

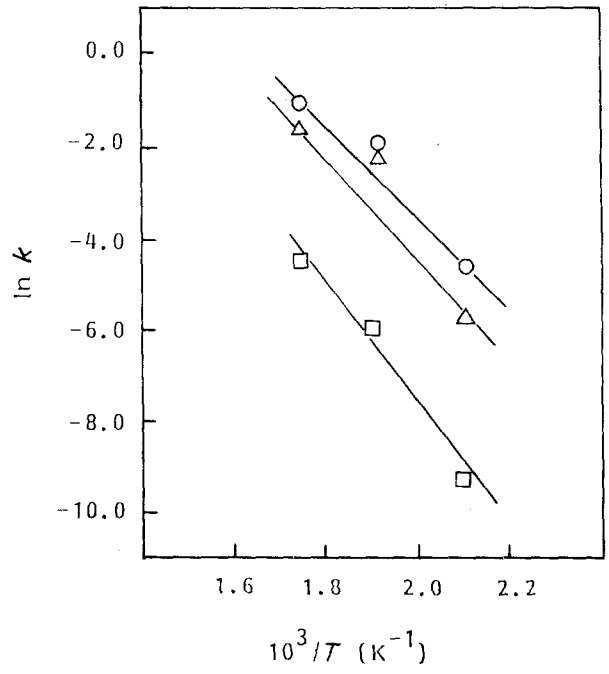

formation of a product layer containing grain-boundary phase and hydrated silica.

2. The rate of hydrothermal corrosion of Si_3N_4 ceramics decreased with decreasing crystallinity of the grain-boundary phase.

3. The corrosion data could be adequately described by the parabolic plot in the initial stage of the reaction.

4. The apparent activation energies were 83.5–108 kJ mol^{-1}, which was almost the same as that of the diffusion of H_2O through amorphous silica.

Figure 7 Arrhenius plots of the rate constants of hydrothermal corrosion of various Si_3N_4 ceramics. (○) SN–1, (△) SN–2, (□) SN–3.

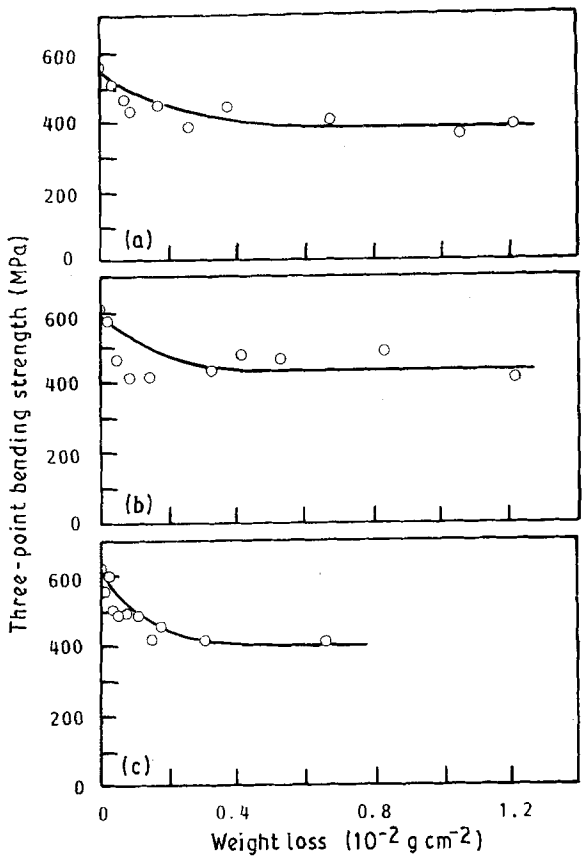

Figure 8 The bending strength of various Si_3N_4 ceramics corroded under hydrothermal conditions at 200–300 °C as a function of weight loss. (a) SN-1, (b) SN-2, (c) SN-3.

5. The bending strength of the corroded samples decreased from ~ 600–400 MPa in the initial stage of the reaction until causing weight loss of 0.004 g cm^{-2} and then were almost constant up to 0.012 g cm^{-2} weight loss.

References

1. A. TSUGE, K. NISHIDA and M. KOMATSU, *J. Amer. Ceram. Soc.* **58** (1975) 323.
2. T. SATO, Y. TOKUNAGA, T. ENDO, M. SHIMADA, K. KOMEYA, K. NISHIDA, M. KOMATSU and T. KAMEDA, *J. Mater. Sci.* **23** (1988) 3440.
3. T. SATO, Y. TOKUNAGA, T. ENDO, M. SHIMADA, K. KOMEYA, M. KOMATSU and T. KAMEDA, *J. Amer. Ceram. Soc.* **71** (1988) 1074.
4. M. YOSHIMURA, J. KASE and S. SOMIYA, *Yogyo Kyokai-Shi* **94** (1986) 129.
5. C. CONTET, J. KASE, T. NOMA, M. YOSHIMURA and S. SOMIYA, *J. Mater. Sci. Lett.* **6** (1987) 963.
6. T. YOSHIO, K. ODA, K. O-OKA and K. ODA, *Yogyo Kyokai-Shi* **94** (1986) 116.
7. T. YOSHIO, K. ODA and K. ODA, *ibid.* **95** (1987) 435.
8. T. YOSHIO and K. ODA, *ibid.* **95** (1987) 730.
9. L. L. HENCH, *J. Non-Cryst. Solids* **25** (1977) 343.
10. M. L. HAIR, "Infrared Spectroscopy in Surface Chemistry" (Marcel Dekker, New York, 1967) p. 173.
11. I. BURN and J. P. ROBERTS, *Phys. Chem. Glasses* **11** (1970) 106.

Received 27 November 1989
and accepted 18 July 1990